Hindawi
Modelling and Simulation in Engineering
Volume 2017, Article ID 3012949, 8 pages
https://doi.org/10.1155/2017/3012949

Research Article

Numerical Analysis of Joule Heating Behavior and Residual Compressive Stress around Crack Tip under High Electric Load

Thomas Jin-Chee Liu

Department of Mechanical Engineering, Ming Chi University of Technology, Taishan, New Taipei City, Taiwan

Correspondence should be addressed to Thomas Jin-Chee Liu; jinchee@mail.mcut.edu.tw

Received 20 July 2017; Accepted 14 September 2017; Published 19 October 2017

Academic Editor: Dimitrios E. Manolakos

This paper discusses the Joule heating effect and residual compressive stress near the crack tip under the electro-thermo-structural coupling state. For the crack tip field, the compressive condition is important for retarding or stopping the crack growth.

1. Introduction

The Joule heating behavior and electro-thermo-structural coupled-field around the crack tip were firstly investigated and discussed by Russian scholars in the 1980s [1, 2]. They used mathematical methods to analyze the crack-tip field under the electric current. Following their pioneer research, many typical studies were done for solving this problem in the last decades [3–12].

Based on the past references, the Joule heating phenomenon near the crack tip is well known. Figure 1 illustrates the concept of this problem. Due to the Joule heating effect, the thermoelectric phenomenon occurs in the conductive material under the electric load. In other words, the material gets hotter when it is subjected to the electric current. If the material has cracks or fractures, the electric current density concentration occurs around the crack tip. Then this electric concentration causes a local hot region at the crack tip due to the Joule heating. In addition, the electric current density has $r^{-1/2}$ singularity at the crack tip [6]. This is similar to the elastic stress field.

Under the Joule heating, the compressive stresses can be produced around the crack tip [1, 2]. This crack-tip compressive stress field is important to reduce or stop the potential crack growth. However, the past references did not show the time-history of the crack-tip stress. During the electric loading, unloading, and cooling process, the crack-tip stress may present the tensile or compressive state. If the plastic strain or deformation occurs at high temperature, the residual stress around the crack tip will be an important topic for the fracture problem.

In this paper, the Joule heating behavior and residual stress around the crack tip will be investigated using the electro-thermo-structural coupling finite element analysis. The temperature and electric current density fields will be also obtained for estimating the crack tip behavior. In particular, this primary study will discuss the residual compressive stress and its importance for stopping the crack growth.

2. Problem Statement

Figure 2 shows the geometric and loading conditions of the steel plate in this study. The plate with an edge crack is subjected to the constant direct current (DC) i_0. The electric loading time is t_e. The plate is made of the mild steel with the dimension $W \times L \times e$. The crack length is a. This problem will be simulated by the three-dimensional finite element analysis with the solid model.

To consider practical conditions, the temperature-dependent material properties in Table 1 [9, 13] are adopted in the finite element analysis. Also, the elastoplastic material properties as shown in Figure 3 are considered. Under the

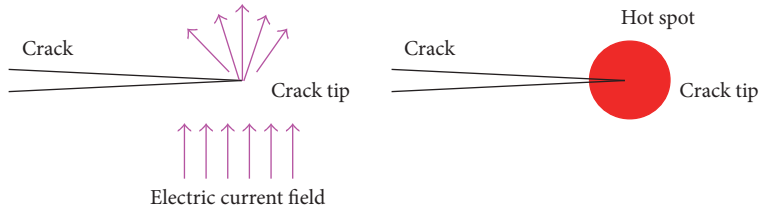

Figure 1: Electric current concentration and hot spot at crack tip.

Table 1: Temperature-dependent physical properties of mild steel [9, 13].

Temperature (°C)	Young's modulus E (GPa)	Yielding strength S_Y (MPa)	Coefficient of thermal expansion α (1/°C)	Thermal conductivity k (W/m-°C)	Specific heat C_p (J/kg-°C)	Resistivity ρ (Ω-m)
21	206.8	248	10.98×10^{-6}	64.60	444	0.14224×10^{-6}
93	196.5	238	11.52×10^{-6}	63.15	452.38	0.18644×10^{-6}
204	194.4	224	12.24×10^{-6}	55.24	511.02	0.26670×10^{-6}
315.5	186	200	12.96×10^{-6}	49.87	561.29	0.37592×10^{-6}
426.7	169	173	13.50×10^{-6}	44.79	611.55	0.49530×10^{-6}
537.8	117	145	14.04×10^{-6}	39.71	661.81	0.64770×10^{-6}
648.9	55	76	14.58×10^{-6}	34.86	762.34	0.81788×10^{-6}
760	6.9	14	14.05×10^{-6}	30.46	1005.3	1.0109×10^{-6}
871	—	—	13.05×10^{-6}	28.37	1005.3	1.1151×10^{-6}
982	—	—	—	27.62	1005.3	1.1582×10^{-6}
1093	—	—	—	28.52	1189.6	1.1786×10^{-6}
1204	—	—	—	—	1189.6	1.2090×10^{-6}

Poisson's ratio $\nu = 0.3$, density $\beta = 7861.2\,\text{kg/m}^3$, melting point = 1521°C.

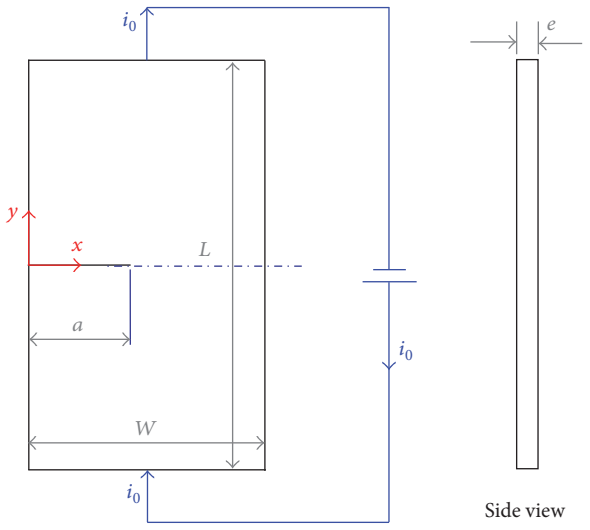

Figure 2: Geometric and loading conditions.

Joule heating effect, the electric-current-induced thermo-structural problem is transient. The initial temperature is 21°C. The convection coefficients on all solid/air interfaces are set as 10 W/m^2-°C.

The contact condition between crack surfaces is considered as the coupled-field problem. The electric current and heat flow can pass through the crack surfaces when the crack contact occurs. The detailed information of the contact condition will be described in the next section.

3. Principles and Finite Element Modelling

3.1. Basic Principles. In this paper, the analysis is the electro-thermo-structural coupled-field problem. First, for the electric current field, it obeys the following equations [14]:

$$\mathbf{E} = -\nabla\phi,$$
$$\mathbf{J} = \frac{1}{\rho}\mathbf{E}, \tag{1}$$
$$\nabla \cdot \mathbf{J} = 0,$$

where $\mathbf{E}$, $\mathbf{J}$, ϕ, and ρ are the electric field (V/m), electric current density (A/m^2), electric potential (V), and resistivity (Ω-m), respectively.

For the transient thermal analysis, the rules are as follows [14, 15]:

$$\mathbf{q}'' = -k\nabla T,$$
$$k\nabla^2 T + \dot{q} = \beta C_p \frac{\partial T}{\partial t}, \tag{2}$$
$$\dot{q} = \rho\,|\mathbf{J}|^2,$$

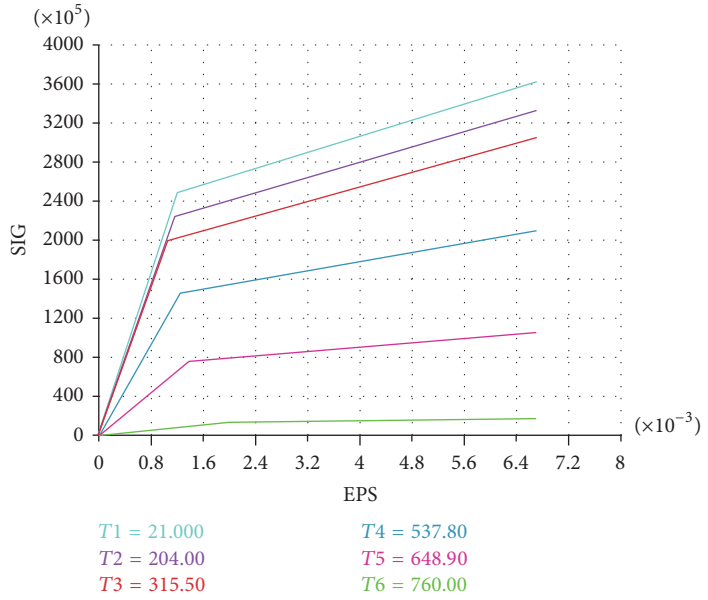

FIGURE 3: Bilinear elastoplastic stress-strain properties (SIG: stress, units: Pa; EPS: strain, dimensionless; $T1$~$T6$: different temperatures, units: °C).

where $\mathbf{q}''$, k, T, $\dot{q}$, β, C_p, and t are the heat flux (W/m^2), thermal conductivity (W/m-°C), temperature (°C), heat generation (W/m^3) of Joule heating, mass density (kg/m^3), specific heat (J/kg-°C), and time (s), respectively.

The thermoelastic analysis couples the thermal and elastic stress fields as follows [16]:

$$\begin{aligned} \sigma_{ji,j} + X_i &= \beta \ddot{u}_i, \quad i, j = x, y, z \\ \varepsilon_{ij} &= \frac{1}{2}\left(u_{i,j} + u_{j,i}\right), \quad i, j = x, y, z \\ \varepsilon_{ij} &= \frac{1}{E}\left[(1+\nu)\,\sigma_{ij} - \left(\nu I_1 - E\alpha\Delta T\right)\delta_{ij}\right], \\ & \qquad\qquad i, j = x, y, z, \end{aligned} \tag{3}$$

where σ_{ij}, ε_{ij}, X_i, u_i, $\ddot{u}_i$, E, ν, I_1, α, ΔT, and δ_{ij} are the stress (Pa = N/m^2), strain (dimensionless), body force (N/m^3), displacement (m), acceleration (m/s^2), Young's modulus (Pa), Poisson's ratio (dimensionless), stress invariant ($I_1 = \sigma_{xx} + \sigma_{yy} + \sigma_{zz}$), coefficient of thermal expansion (1/°C), temperature difference ($\Delta T = T - T_0$ where T_0 is the reference temperature) and Kronecker delta, respectively.

In this study, the elastoplastic stress-strain behavior is considered. The von Mises yield criterion [17, 18] is used to analyze the plastic stress and strain. The yield surface is defined as

$$\sigma_{\text{eqv}} = S_Y \tag{4a}$$

$$\sigma_{\text{eqv}} = \sqrt{\frac{1}{2}\left[(\sigma_1 - \sigma_2)^2 + (\sigma_1 - \sigma_3)^2 + (\sigma_3 - \sigma_2)^2\right]}, \tag{4b}$$

where S_Y, σ_{eqv}, and σ_i ($i = 1, 2, 3$) are the yielding strength, von Mises equivalent stress, and principal stress, respectively. In this study, the stress-strain relationships in Figure 3 are used.

The finite element equations of the electro-thermo-structural coupled-field analysis are as follows [18]:

$$\begin{aligned} &\begin{bmatrix} \mathbf{M} & 0 & 0 \\ 0 & 0 & 0 \\ 0 & 0 & 0 \end{bmatrix} \begin{bmatrix} \ddot{\mathbf{U}} \\ \ddot{\mathbf{T}} \\ \ddot{\mathbf{V}} \end{bmatrix} + \begin{bmatrix} \mathbf{C} & 0 & 0 \\ \mathbf{C^{tu}} & \mathbf{C^{t}} & 0 \\ 0 & 0 & 0 \end{bmatrix} \begin{bmatrix} \dot{\mathbf{U}} \\ \dot{\mathbf{T}} \\ \dot{\mathbf{V}} \end{bmatrix} \\ &+ \begin{bmatrix} \mathbf{K} & \mathbf{K^{ut}} & 0 \\ 0 & \mathbf{K^{t}} & 0 \\ 0 & 0 & \mathbf{K^{v}} \end{bmatrix} \begin{bmatrix} \mathbf{U} \\ \mathbf{T} \\ \mathbf{V} \end{bmatrix} = \begin{bmatrix} \mathbf{F} \\ \mathbf{Q} \\ \mathbf{I} \end{bmatrix}, \end{aligned} \tag{5}$$

where $\mathbf{U}$, $\mathbf{T}$, $\mathbf{V}$, $\mathbf{F}$, $\mathbf{Q}$, and $\mathbf{I}$ are the vector forms of the displacement, temperature, electric potential, force, heat flow rate, and electric current, respectively. The material constant matrices $\mathbf{M}$, $\mathbf{C}$, $\mathbf{C^t}$, $\mathbf{C^{tu}}$, $\mathbf{K}$, $\mathbf{K^t}$, $\mathbf{K^{ut}}$, and $\mathbf{K^v}$ are the structural mass, structural damping, thermal specific heat, thermo-structural damping, structural stiffness, thermal conductivity, thermo-structural stiffness, and electric conductivity, respectively. The coupled heat flow matrix $\mathbf{Q}$ contains the effects of the thermal loading and Joule heating. $\mathbf{C^{tu}}$ and $\mathbf{K^{ut}}$ are thermo-structural coupled terms. Equation (5) is a directly coupled nonlinear equation which is solved using the Newton-Raphson iterative method [18].

3.2. Boundary and Initial Conditions. Referring to Figure 2, the boundary and initial conditions are listed as follows:

$$J\left(x, -\frac{L}{2}, t\right) = \frac{i_0(t)}{(eW)},$$

$$\phi\left(x, \frac{L}{2}, t\right) = 0,$$

$$0 \le x \le W$$

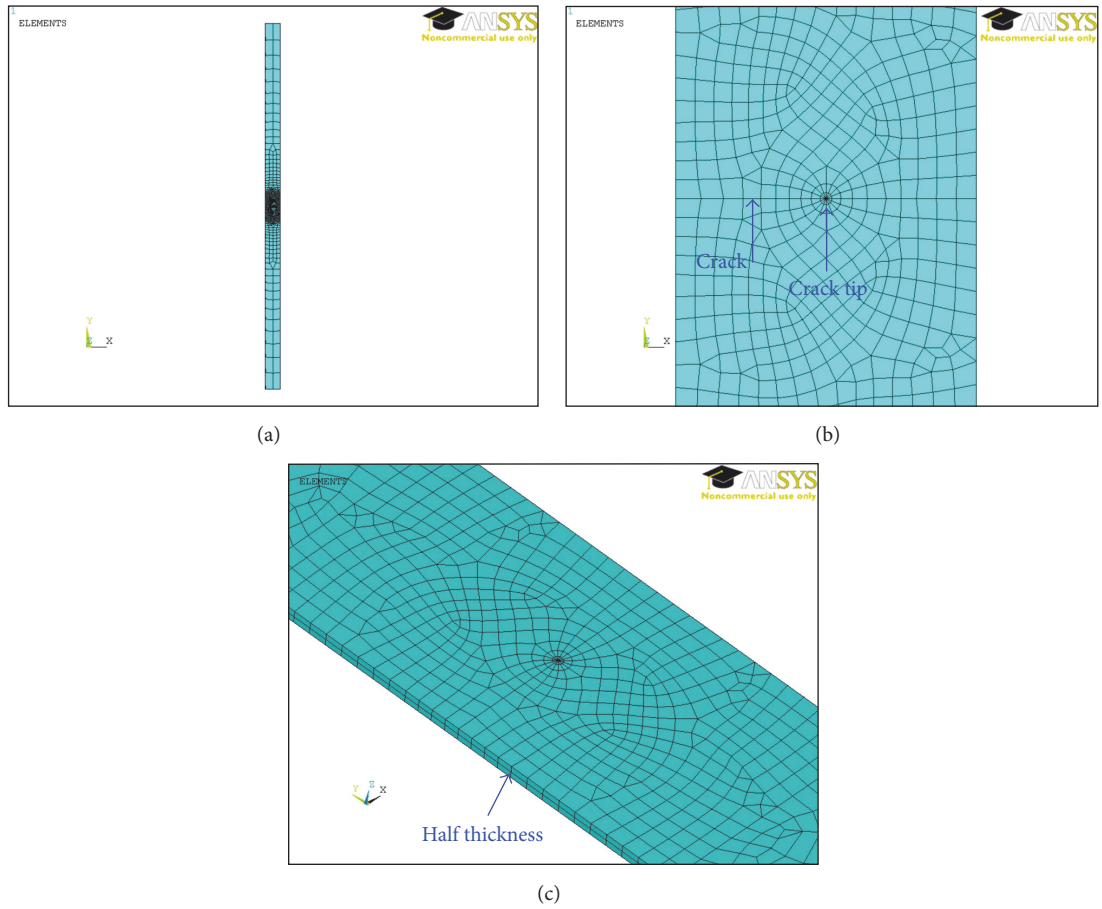

FIGURE 4: Finite element model. (a) Entire view of plate, (b) local region near crack, and (c) three-dimensional view.

$$T(x, y, 0) = T_0 = 21^{\circ}\mathrm{C}$$
$$u_i(x, y, 0) = \dot{u}_i(x, y, 0) = \ddot{u}_i(x, y, 0) = 0. \tag{6}$$

The convective heat transfer on all structure/air interfaces is considered. The convection condition $h = 10\,\mathrm{W/m^2\text{-}^{\circ}C}$ and $T_\infty = 21^{\circ}\mathrm{C}$ is applied.

3.3. Finite Element Modelling. The software ANSYS is adopted to perform the finite element modelling and calculation. In Figure 4, it shows the finite element model of the steel plate with the typical dimensions: $L = 240$ mm, $W = 10$ mm, $e = 1$ mm, and $a = 5$ mm. The mesh is constructed by the 20-node solid element SOLID226 which has the capability of the electro-thermo-structural coupled-field analysis. Due to the symmetry, only half thickness is analyzed. In addition, the quarter-point elements are used to simulate the $r^{-1/2}$ singularity at the crack tip [9–12, 19].

3.4. Contact Condition on Crack Surfaces. The electro-thermo-structural contact condition on both crack surfaces is considered in the numerical analysis. In ANSYS, two contact element types, TARGE170 and CONTA174, are adopted. Aside from the contact stress, the electric and thermal contacts are considered as the following equations [18, 20]:

$$J = \eta_{\mathrm{cel}}(\phi_1 - \phi_2)$$
$$q'' = \eta_{\mathrm{cth}}(T_1 - T_2), \tag{7}$$

where η_{cel} and η_{cth} are, respectively, the electric conductance and thermal conductance of the contact surfaces. The terms $(\phi_1 - \phi_2)$ and $(T_1 - T_2)$ are, respectively, the electric potential difference and temperature difference between both contact surfaces. In this study, η_{cth} is assumed to be very large so that the thermal contact resistance on crack surfaces can be ignored. However, η_{cel} is defined as follows [20]:

$$\eta_{\mathrm{cel}} = \frac{1}{\rho_c l_c}, \tag{8}$$

where ρ_c and l_c are the electric contact resistivity and characteristic length, respectively. For mild steel, the typical values $\eta_{\mathrm{cel}} = 6.29 \times 10^8\ 1/(\Omega\mathrm{m}^2)$, $\rho_c = 6.2586 \times 10^{-5}\ \Omega\mathrm{m}$, and $l_c = 2.54 \times 10^{-5}$ m (0.001 inch) [13] are used. In addition, the coefficient of friction on crack surfaces is neglected.

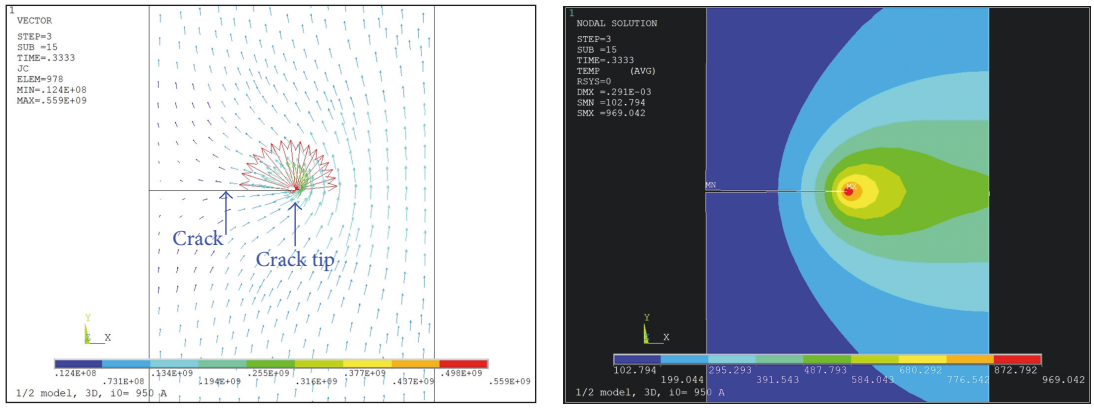

(a) (b)

Figure 5: (a) Electric current density field (units: A/m^2). (b) Temperature field (units: ˚C).

4. Results and Discussions

4.1. Validation of Finite Element Model. The accuracy of the finite element model must be valid. For the validation, the coupled-field analysis is simplified to the pure electric problem. Furthermore, the SOLID226 elements are degenerated to SOLID231 elements for the ANSYS model in Figure 4. In this case, the resistivity is $7.2 * 10^{-7}$ Ω-m. Also, the distributed current $J_0 = 6.25 * 10^6$ A/m^2 is used to replace the concentrated current i_0.

Using the limited electric potential extrapolation technique (LEPET) [9], the electric current density factor K_J at the crack tip can be obtained from the finite element results. In this case, the numerical result of K_J is $8.857 * 10^5$ Am$^{-3/2}$. According to the analogy and analytical methods [8, 9, 21], the analytical solution of the edge crack problem under electric load J_0 is

$$K_J = BJ_0\sqrt{\pi a}, \tag{9}$$

where $B = 1.128$ for the case of $a/W = 0.5$. Substituting all values to (9), K_J is $8.836 * 10^5$ Am$^{-3/2}$. By comparing both values of K_J, the finite element result has good agreement with the analytical solution with the small numerical error 0.24%.

4.2. Electric Concentration and Hot Spot at Crack Tip. The Joule heating effect makes high temperature field in the steel plate. Due to the local electric concentration at the crack tip, a hot spot exists. In Figure 5, it shows the electric current density and temperature fields around the crack under the following conditions: $L = 240$ mm, $W = 10$ mm, $e = 1$ mm, $a = 5$ mm, and $i_0 = 950$ A. The electric loading time is $t_e = 0.3333$ s. The numerical results obviously prove the phenomena of the electric concentration and hot spot at the crack tip.

4.3. Residual Compressive Stress at Crack Tip. In this section, the geometric and loading conditions of the steel plate are the same as the above section. As shown in Figure 6, the unloading and cooling processes are added in the analysis to obtain the residual stress around the crack tip. The loading process is during $t = 0$~0.3333 s. Then the electric current is removed and it remains the cooling process till $t = 600$ s.

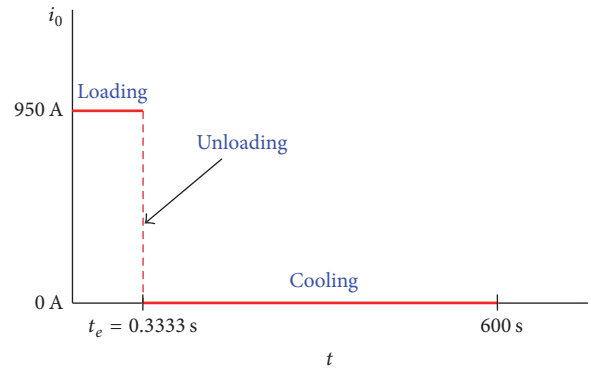

Figure 6: Electric loading, unloading, and cooling history.

In Figure 7, the time-history of the crack tip temperature is shown. It can be seen that the crack tip temperature reaches the maximum value (969˚C) at the end of the loading time ($t_e = 0.3333$ s). After the unloading process, the temperature decays quickly and approaches the steady state. At $t = 600$ s, the crack tip temperature decreases to 25˚C.

Figures 8–10 show the time-history of the normal stress σ_y at the point B near the crack tip. The distance from B to the crack tip is 0.2 mm. In Figure 8, it shows the negative values of σ_y during the cooling process till $t = 600$ s. Also, it approaches the steady state. At $t = 600$ s, the value of σ_y is −301 MPa. The negative value implies the compressive normal stress. In other words, the residual compressive stress exists near the crack tip after the electric load is removed.

In Figures 9 and 10, the detailed stress values during shorter time intervals are shown. The stress causes complicated fluctuation during the electric loading and unloading processes. Then it decays and approaches the steady state with sufficient cooling time.

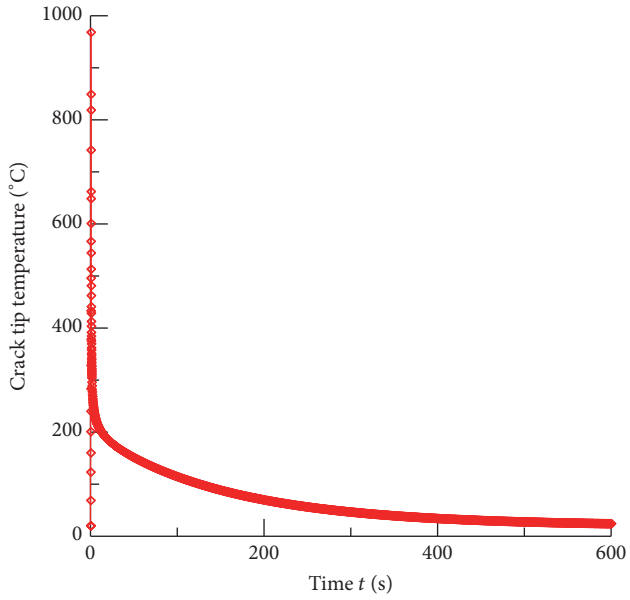

FIGURE 7: Time-history of crack tip temperature (t = 0~600 s).

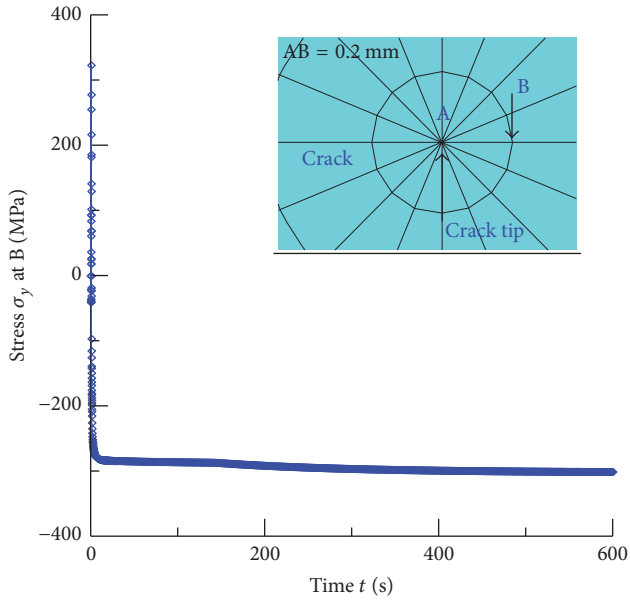

FIGURE 8: Time-history of stress near crack tip (t = 0~600 s).

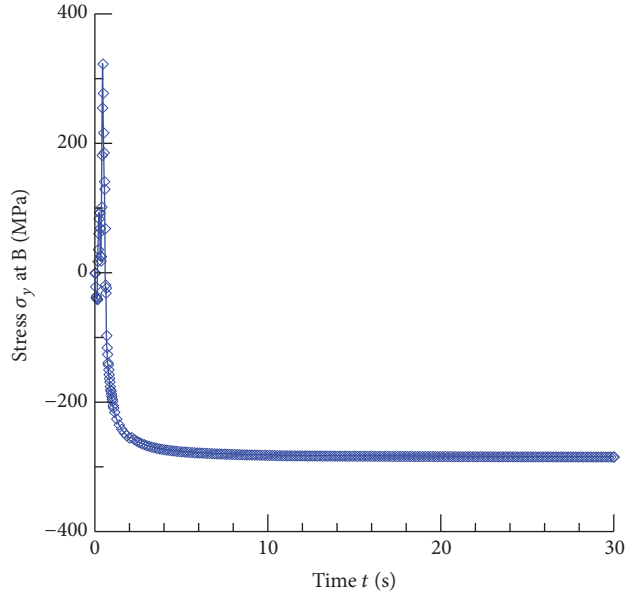

FIGURE 9: Time-history of stress near crack tip (t = 0~30 s).

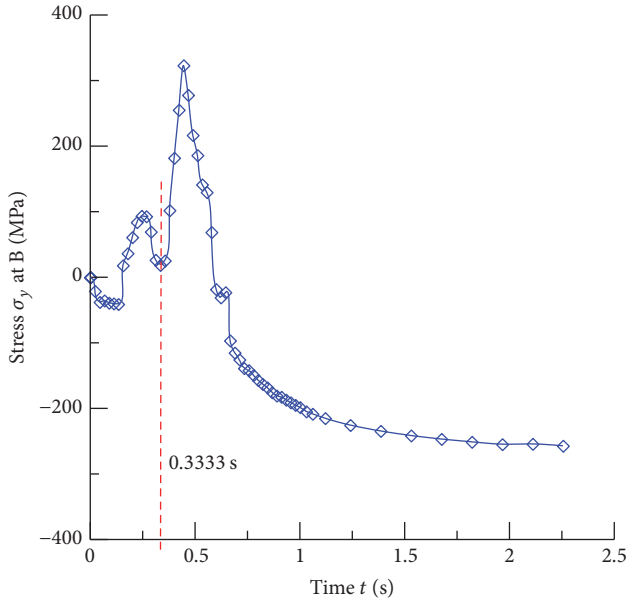

FIGURE 10: Time-history of stress near crack tip (t = 0~2.5 s).

Figure 11 shows the contour of the stress σ_y near the crack tip at the end of the cooling process (t = 600 s). There are negative stress values around the crack tip. It means that the residual compressive stresses occur in this area. According to the results of Figure 11, Figure 12 shows the stress distribution in front to the crack tip. The compressive stress field is also investigated near the crack tip.

4.4. Effects of Electric Load. Figure 13 shows the time-history of the stress at point B under i_0 = 950 A and i_0 = 400 A. Comparing two curves in the figure, it is found that there is no residual stress under i_0 = 400 A. It implies that the magnitude of the electric load is an important parameter for producing the residual compressive stress near the crack tip. If the electric load is not sufficient, the temperature and stress will be too small to make the yielding (plastic) strain and residual stress.

5. Conclusions

From the finite element results, the electric current density concentrates at the crack tip. Due to the Joule heating, it causes a hot spot at the crack tip. The residual compressive stress appears near the crack tip due to the high temperature

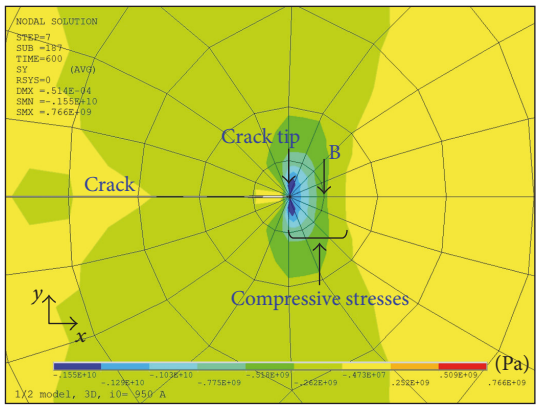

Figure 11: Contour of stress σ_y near crack tip (t = 600 s).

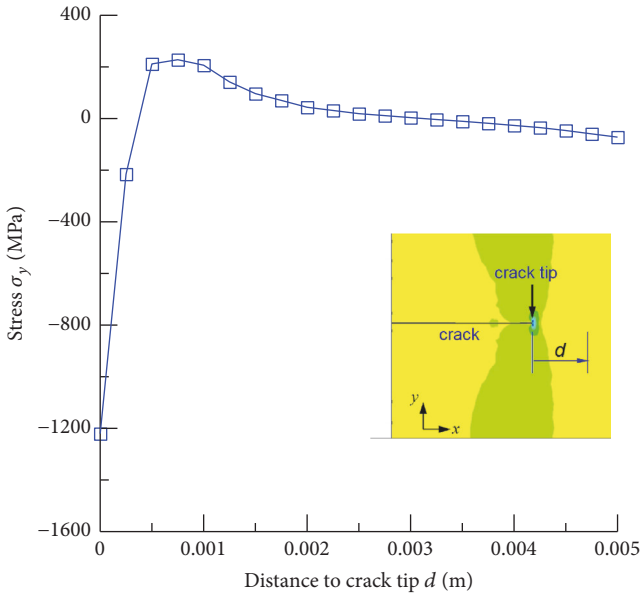

Figure 12: Stress distribution in front to crack tip (t = 600 s).

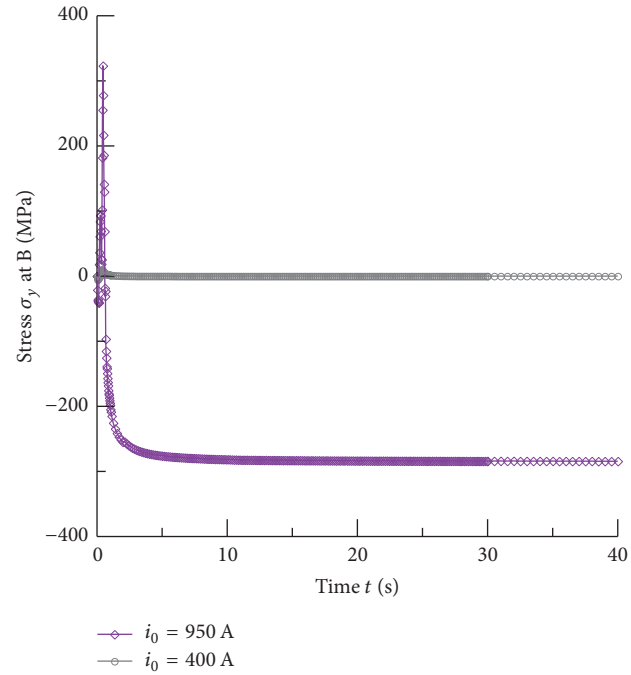

Figure 13: Time-history of stress near crack tip under different electric loads.

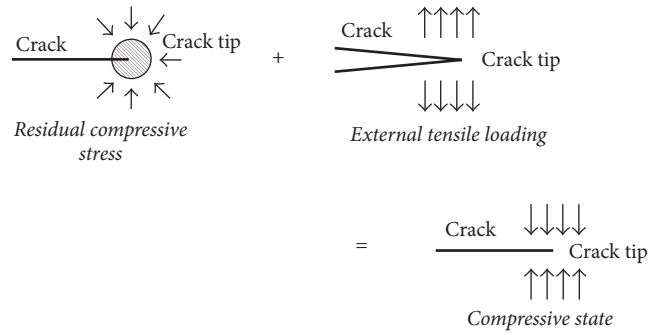

Figure 14: Concept for stopping crack growth.

and plastic deformation. Furthermore, the compressive condition can retard or stop the crack growth. The concept for stopping crack growth is shown in Figure 14.

This paper provides a primary study and conclusion of the residual compressive stress near the crack tip under the electro-thermo-structural coupling state. The compressive condition is practically important to the fracture mechanics problem.

It is important to study the fatigue crack growth due to the Joule heating caused stresses. The extending work will be considered in the future research.

Nomenclature

i_0: Electric load (direct current, DC) (A)
t: Time (s)
t_e: Electric loading time (s)
W, L, e: Plate dimensions (m)
a: Crack length (m)
C_p: Specific heat (J/kg-°C)
T, $\mathbf{T}$: Temperature (°C)
β: Mass density (kg/m^3)
$\mathbf{E}$: Electric field (V/m)
J_i, $\mathbf{J}$: Electric current density (A/m^2)
ϕ, $\mathbf{V}$: Electric potential (V)
ρ: Resistivity (Ω-m)
$\mathbf{q}''$: Heat flux (W/m^2)
k: Thermal conductivity (W/m-°C)
$\dot{q}$: Heat generation of Joule heating (W/m^3)
σ_{ij}: Stress (Pa)
ε_{ij}: Strain (dimensionless)
u_i, $\mathbf{U}$: Displacement (m)
E: Young's modulus (Pa)
ν: Poisson's ratio (dimensionless)
α: Coefficient of thermal expansion (1/°C)

T_0: Reference temperature (°C)
S_Y: Yielding strength (Pa)
σ_{eqv}: von Mises equivalent stress (Pa)
F: Force (N)
Q: Heat flow rate (W)
I: Electric current (A)
h: Coefficient of convection (W/m^2-°C)
T_∞: Ambient temperature (°C)
η_{cel}: Electric conductance of contact surface ($m^{-2}\Omega^{-1}$)
η_{cth}: Thermal conductance of contact surface (W/m^2-°C)
ρ_c: Contact resistivity of contact surface (Ω-m).

Conflicts of Interest

The author declares that there are no conflicts of interest.

Acknowledgments

The author would like to acknowledge the Ministry of Science and Technology in Taiwan for the financial support under Contract nos. MOST 104-2221-E-131-030 and MOST 105-2221-E-131-014.

References

[1] V. Z. Parton and B. A. Kudryavtsev, *Electromagnetoelasticity*, Gordon and Breach, New York, NY, USA, 1988.

[2] B. A. Kudryavtsev, V. Z. Parton, and B. D. Rubinskii, "Electromagnetic and thermoelastic fields in a conducting plate with a cut of finite length," *Mechanics of Solids*, vol. 17, pp. 110–118, 1982.

[3] D. Hasanyan, L. Librescu, Z. Qin, and R. D. Young, "Thermoelastic cracked plates carrying nonstationary electrical current," *Journal of Thermal Stresses*, vol. 28, no. 6-7, pp. 729–745, 2005.

[4] Z. Qin, L. Librescu, and D. Hasanyan, "Joule heating and its implications on crack detection/arrest in electrically conductive circular cylindrical shells," *Journal of Thermal Stresses*, vol. 30, no. 6, pp. 623–637, 2007.

[5] G. X. Cai and F. G. Yuan, "Electric current-induced stresses at the crack tip in conductors," *International Journal of Fracture*, vol. 96, pp. 279–301, 1996.

[6] G. X. Cai and F. G. Yuan, "Stresses around the crack tip due to electric current and self-induced magnetic field," *Advances in Engineering Software*, vol. 29, no. 3-6, pp. 297–306, 1998.

[7] F. u. YM, X. Z. Bai, G. Y. Qiao, H. u. YD, and J. Y. Luan, "Technique for producing crack arrest by electromagnetic heating," *Materials Science and Technology*, vol. 17, pp. 1653–2656, 2001.

[8] X. Z. Bai, Z. G. Tian, and J. Zheng, *Thermo-electric effects in fracture mechanics*, National Defense Industry Press, China, 2009.

[9] T. J. C. Liu, "Thermo-electro-structural coupled analyses of crack arrest by Joule heating," *Theoretical and Applied Fracture Mechanics*, vol. 49, no. 2, pp. 171–184, 2008.

[10] T. J. C. Liu, "Finite element modeling of melting crack tip under thermo-electric Joule heating," *Engineering Fracture Mechanics*, vol. 78, no. 4, pp. 666–684, 2011.

[11] T. J. C. Liu, "Crack detection/arrest with Joule heating," in *Encyclopedia of Thermal Stresses*, R. B. Hetnarski, Ed., Springer Science + Business Media Dordrecht, Dordrecht, Netherlands, 2013.

[12] T. J.-C. Liu, "Joule heating behaviors around through crack emanating from circular hole under electric load," *Engineering Fracture Mechanics*, vol. 123, pp. 2–20, 2014.

[13] C. L. Tsai, W. L. Dai, and D. W. Dickinson, "Analysis and development of a real-time control methodology in resistance spot welding," *Welding Journal*, vol. 70, pp. s339–s351, 1991.

[14] D. K. Cheng, *Field and Wave Electromagnetics*, Addison-Wesley, MA, USA, 1983.

[15] F. P. Incropera and D. P. DeWitt, *Fundamentals of Heat and Mass Transfer*, John Wiley & Sons, 5th edition, 2002.

[16] A. P. Boresi and K. P. Chong, *Elasticity in Engineering Mechanics*, John Wiley & Sons, New York, NY, USA, 2nd edition, 2000.

[17] O. C. Zienkiewicz and R. L. Taylor, *The Finite Element Method*, vol. 2, McGraw-Hill, New York, 4th edition, 1991.

[18] ANSYS Inc., *ANSYS 16.2 Mechanical APDL Theory Reference*, SAS IP, 2015.

[19] R. S. Barsoum, "On the use of isoparametric finite elements in linear fracture mechanics," *International Journal for Numerical Methods in Engineering*, vol. 10, no. 1, pp. 25–37, 1976.

[20] X. Sun and P. Dong, "Analysis of aluminum resistance spot welding processes using coupled finite element procedures," *Welding Journal*, vol. 79, pp. s215–s221, 2000.

[21] G. C. Sih, *Handbook of Stress Intensity Factors*, Lehigh University, Pennsylvania, Pa, USA, 1973.